Scattering Studies of the Structure of Colloid–Polymer Suspensions and Gels

ARTICLE *in* LANGMUIR · JUNE 2003

Impact Factor: 4.46 · DOI: 10.1021/La020982g

5 AUTHORS, INCLUDING:

Yeng-Long Chen
Academia Sinica
68 PUBLICATIONS **1,095** CITATIONS
SEE PROFILE

Charles Zukoski
University at Buffalo, The State University of…
208 PUBLICATIONS **8,942** CITATIONS
SEE PROFILE

Scattering Studies of the Structure of Colloid−Polymer Suspensions and Gels

S. A. Shah, S. Ramakrishnan, Y. L. Chen, K. S. Schweizer,* and C. F. Zukoski*

Departments of Chemical and Biomolecular Engineering and Materials Science and Engineering and Materials Research Laboratory, University of Illinois, Urbana, Illinois 61801

Received December 23, 2002. In Final Form: March 19, 2003

Depletion-driven changes in the structure of hard-sphere particles (radius R) mixed with a nonadsorbing polymer (radius of gyration R_g) dissolved in good (athermal) and ideal (theta) solvents are systematically studied. Colloidal structure factors, $S(q)$, are determined using slit-smeared and pinhole-collimated ultra-small-angle X-ray scattering and small-angle neutron scattering. A comparison of the structure factors extracted from the three methods demonstrates the validity of the available desmearing algorithms. Polymer additives alter the colloidal structure more for larger particle volume fractions (ϕ_c) and smaller size asymmetry ratios R_g/R. At fixed $\phi_c \sim 0.40$ and $R_g/R = 0.06$, increasing the reduced polymer concentration (c_p/c_p^*) results in a monotonic shift to higher wavevectors of the location of the first peak in the structure factor, q^*, and a nonmonotonic variation of the cage order parameter, $S(q^*)$, in a nearly solvent quality independent manner. Local structural correlations arrest as the gel state is entered. The reduced polymer concentration required for gelation is smaller in athermal solvents compared to its theta analogue and, in both cases, is well below the fluid−fluid spinodal boundaries. Comparisons between the measured structure factors and no-adjustable-parameter predictions of the polymer reference interaction site model theory shows near quantitative agreement over all wavevectors. When the gel phase is entered, strong differences between the theory and the experiment emerge, indicating the nonequilibrium nature of structural correlations in the nonergodic gel. Relative to equilibrium expectations, enhanced (reduced) fluctuations occur at small (intermediate) wavevectors. The combined experimental and theoretical results suggest that neither long wavelength fluctuations nor the local cage structure are the primary origin of the gelation transition.

I. Introduction

As the strength of attraction between colloidal particles is increased, a series of equilibrium or nonequilibrium transitions can occur including fluid−fluid (F−F) and fluid−crystal (F−C) phase separation, gelation, and vitrification.[1−4] The detailed nature and existence of these transitions are sensitive to both the strength and spatial range of the effective attraction. For homogeneous particles of diameter D interacting via an effective attraction of range Δ, nonequilibrium gelation is often the first transition that occurs if $\Delta/D < 0.1$, F−C if $0.1 < \Delta/D < 0.3$, and F−F if $\Delta/D > 0.3$.[2,4] Several statistical thermodynamic theories have successfully explained the change in equilibrium behavior from F−C to F−F with an increasing spatial range of the attraction and, under certain conditions, the possibility of F−F−C three-phase coexistence.[5,6]

One system that allows both the range and the strength of the effective attraction to be delicately controlled is mixtures of hard-sphere colloids and a nonabsorbing polymer. This attraction arises from the entropy-driven exclusion of the polymers from the regions between the particles.[7] Under dilute polymer concentration conditions, the depletion attraction has a range proportional to the macromolecule radius of gyration and a strength sensitive to both the polymer concentration and the solvent quality. Recent experimental studies[4,8,9] discovered that fundamental errors are incurred by classical statistical thermodynamic theories[5−7] for the dependence of F−F phase separation boundaries on polymer−particle size asymmetry, Δ/D, under good and ideal theta-solvent conditions. Theoretical analysis based on a microscopic integral equation approach, the polymer reference interaction site model (PRISM) theory, established the critical importance of taking into account both the internal conformational degrees of freedom of the polymer and the interchain interactions.[4,8−12]

The microstructural consequences of effective attractions between colloidal particles are much more poorly established and understood, and very limited experimental information exists for colloid−polymer mixtures.[13−15] Recently, the collective particle organization, as was quantified by the scattering structure factor, was determined for hard-sphere colloid−polymer suspensions at a triple-coexistence using a novel two-color dynamic light

* Corresponding authors. E-mail: czukoski@uiuc.edu (C.F.Z.); kschweiz@uiuc.edu (K.S.S.).

(1) Anderson, V. J.; Lekkerkerker, H. N. W. *Nature* **2002**, *416*, 811. Poon, W. C. K.; Starrs, L.; Meeker, S. P.; Moussaid, A.; Evans, R. M. L.; Pusey, P. N.; Robins, M. M. *Faraday Discuss.* **1999**, *112*, 143. Verhaegh, N. A. M.; Asnaghi, D.; Lekkerkerker, H. N. W.; Giglio, M.; Cipelletti, L. *Physica A* **1997**, *242*, 104. de Hoog, E. H. A.; Kegel, W. K.; van Blaaderen, A.; Lekkerkerker, H. N. W. *Phys. Rev. E: Stat. Phys., Plasmas, Fluids, Relat. Interdiscip. Top.* **2001**, *64*, 021407−021401.

(2) Ilett, S. M.; Orrock, A.; Poon, W. C. K.; Pusey, P. N. *Phys. Rev. E: Stat. Phys., Plasmas, Fluids, Relat. Interdiscip. Top.* **1995**, *51*, 1344.

(3) Poon, W. C. K. *J. Phys.: Condens. Matter* **2002**, *14*, R859.

(4) Shah, S. A.; Chen, Y. L.; Schweizer, K. S.; Zukoski, C. F. *J. Chem. Phys.* **2003**, *118*, 3350.

(5) Gast, A. P.; Hall, C. K.; Russel, W. B. *J. Colloid Interface Sci.* **1983**, *96*, 251. Vrij, A. *J. Chem. Phys.* **1978**, *69*, 1742.

(6) Lekkerkerker, H. N. W.; Poon, W. C. K.; Pusey, P. N.; Stroobants, A.; Warren, P. B. *Europhys. Lett.* **1992**, *20*, 559.

(7) Asakura, S.; Oosawa, F. *J. Polym. Sci.* **1958**, *33*, 183.

(8) Ramakrishnan, S.; Fuchs, M.; Schweizer, K. S.; Zukoski, C. F. *J. Chem. Phys.* **2002**, *116*, 2201.

(9) Ramakrishnan, S.; Fuchs, M.; Schweizer, K. S.; Zukoski, C. F. *Langmuir* **2002**, *18*, 1082.

(10) Fuchs, M.; Schweizer, K. S. *Europhys. Lett.* **2000**, *51*, 621.

(11) Fuchs, M.; Schweizer, K. S. *Phys. Rev. E: Stat. Phys., Plasmas, Fluids, Relat. Interdiscip. Top.* **2001**, *64*, 021514.

(12) Fuchs, M.; Schweizer, K. S. *J. Phys.: Condens. Matter* **2002**, *14*, R239.

(13) Bartsch, E.; Eckert, T.; Pies, C.; Sillescu, H. *J. Non-Cryst. Solids* **2002**, *307−310*, 802.

(14) Eckert, T.; Bartsch, E. *Phys. Rev. Lett.* **2002**, *89*, 125701.

(15) Ye, X.; Narayanan, T.; Huang, J. S.; Tong, P. *Phys. Rev. Lett.* **1996**, *76*, 4640.

10.1021/la020982g CCC: $25.00
Published on Web 05/09/2003

scattering (DLS) technique.[16] The dense colloidal liquid phase was studied for three values of the polymer−particle size asymmetry ratio $\xi = R_g/R = 0.24$, 0.37, and 0.57 (where R_g and R are the polymer radius of gyration and particle radius, respectively), each at a single (differing) value of polymer concentration and colloid volume fraction (ϕ_c). The local particle packing or cage structure was found to be relatively insensitive to system parameters, but an order-of-magnitude enhancement of the long wavelength concentration fluctuations were observed, which are larger as ξ decreases. The latter observation is in poor agreement with predictions of the free-volume theory[6] as a result of simplifying the assumptions of treating a polymer as a phantom sphere, but it is in quantitative agreement with the no-adjustable-parameter predictions of the PRISM theory.[10,12]

Knowledge of the influence of polymer additives on the colloidal structure is essential for understanding and controlling the rheological and flow properties, glass formation, and gelation of colloid−polymer suspensions, which are important in many technological applications.[2,13,14,17−20] However, systematic experimental measurements of the depletion-driven structural reorganization of the model hard-sphere colloids on the length scales important for the dynamics are nearly nonexistent.

This paper studies the collective colloidal structure in the fluid and gel states using both synchrotron ultra-small-angle X-ray scattering (USAXS; slit-smeared and pinhole-collimated) and small-angle neutron scattering (SANS). Excellent quantitative agreement is demonstrated between the different scattering methods. We also carry out quantitative, no-adjustable-parameter comparisons with the predictions of the PRISM theory for variable polymer concentrations, size asymmetry ratios, volume fractions, and solvent qualities.

II. Experimental Section

A. Sample Preparation. The silica particles were prepared by the base-catalyzed hydrolysis and condensation of tetra ethyl orthosilicate and seeded growth according to the method of Stober et al.[21] and Bogush et al.[22] The particles were then rendered hydrophobic via the method of van Helden et al.[23] The particles were sized using transmission electron microscopy (TEM; Philips CM-12) and DLS (Brookhaven Instruments BI-200 SM goniometer), and the mean particle diameters compared well with the values determined from small-angle X-ray scattering.

Particles of radius $R = 50$ and 59 nm (each with a standard deviation of ±3 nm, estimated from sizing ~500 particles using TEM) were made to achieve the desired range for the polymer−particle size asymmetry ratio. A known mass of the vacuum-dried silica powder was then suspended in either a 50:50 mixture of *cis*- and *trans*-decalin or toluene and vigorously stirred to disperse the particles. Henceforth, the nomenclature for the solvent used is denoted by the superscripts D (decalin) and T (toluene).

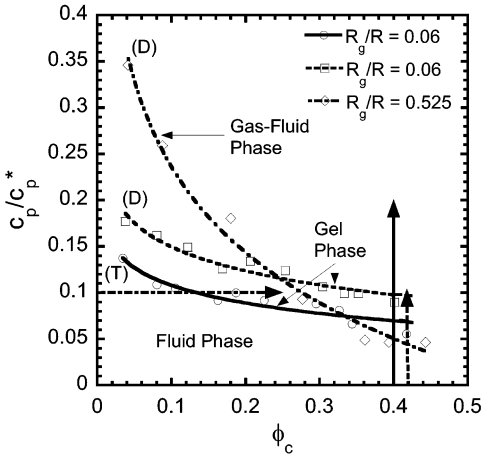

Figure 1. Experimental phase boundaries (gel or gas−fluid) for the sterically stabilized octadecyl silica particles and polystyrene suspended in decalin (D) and toluene (T).[4] The data points are shown along with smooth curves drawn to guide the eye. (Solid) $R_g^T/R = 0.06$, gel; (dashed) $R_g^D/R = 0.06$, gel; (dotted−dashed) $R_g^D/R = 0.525$, gas−fluid, where the superscript denotes the solvent. The arrows designate the direction and extent of the phase diagram explored by the scattering measurements for the different cases.

With the use of the gravimetrically determined density[8,9] of $\rho_c = 1.9 \pm 0.04$ g/cm^3, stock suspensions of a known colloid volume fraction were prepared. The osmotic compressibility[4,8] measurements in the absence of the polymer are in excellent agreement with predictions of the Carnahan−Starling equation of state,[24] confirming that the particles are hard spheres up to $\phi_c \approx 0.45$.[17]

Polystyrene standards of molecular weights $M_w = 1.32 \times 10^4$ and 9.94×10^5 g/mol were purchased from the Sigma−Aldrich Chemical Co. Each has a narrow size distribution with a ratio of the weight-average molecular weight to the number-average molecular weight being less than 1.05. To within the experimental uncertainties, static light scattering measurements show that ideal theta-solvent behavior is observed ($R_g^D \propto M_w^{1/2}$), in accordance with previous studies.[25] This scaling is used to determine the radii of gyration and the dilute−semidilute-overlap-concentration (c_p^*) values for the smaller-molecular-weight polymer used in this study and as were previously reported.[4] The good solvent scaling law in toluene ($R_g^T \propto M_w^{3/5}$) is used to determine R_g^T.[26]

The structural changes in suspensions experiencing relatively long-range depletion interactions are briefly studied for particles suspended in decalin and $R_g/R = 0.525$ ($M_w = 9.94 \times 10^5$ g/mol). F−F demixing is observed at elevated polymer concentrations.[4] Measurements were made at a fixed dimensionless polymer concentration ($c_p/c_p^* = 0.1$) with varying colloid volume fractions ($\phi_c = 0.25$ and 0.08 ± 0.01) in the homogeneous phase, effectively traversing horizontally through the phase diagram shown in Figure 1.

A second series of studies focuses on the effects of increasing the strength of the depletion attractions by varying the dimensionless polymer concentration at a high volume fraction and small size asymmetry ratio. For studies in the near-theta solvent decalin, $\phi_c = 0.42 \pm 0.01$ and $R_g/R = 0.061$ ($M_w = 1.32 \times 10^4$ g/mol). For this system, gelation is observed at $c_p/c_p^* = 0.095 \pm 0.005$ and preempts an equilibrium phase transition. The colloid and polymer stock solutions were initially prepared such that the suspensions were in the homogeneous fluid phase, and the gel boundary was accessed by traversing vertically through the phase diagram, as is shown in Figure 1.

(16) Moussaid, A.; Poon, W. C. K.; Pusey, P. N.; Soliva, M. F. *Phys. Rev. Lett.* **1999**, *82*, 225.
(17) Russel, W. B.; Saville, D. A.; Schowalter, W. R. *Colloidal Dispersions*; Cambridge University Press: Cambridge, U.K., 1989.
(18) Napper, D. H. *Polymeric Stabilization of Colloidal Dispersions*; Academic Press: New York, 1983.
(19) Pham, K. N.; Puertas, A. M.; Bergenholtz, J.; Egelhaaf, S. U.; Moussaid, A.; Pusey, P. N.; Schofield, A. B.; Cates, M. E.; Fuchs, M.; Poon, W. C. K. *Science* **2002**, *296*, 104. Bergenholtz, J.; Fuchs, M. *Phys. Rev. E: Stat. Phys., Plasmas, Fluids, Relat. Interdiscip. Top.* **1999**, *59*, 5706.
(20) Bergenholtz, J.; Fuchs, M.; Voigtmann, T. *J. Phys.: Condens. Matter* **2000**, *12*, 6575. Dawson, K.; Foffi, G.; Fuchs, M.; Gotze, W.; Sciortino, F.; Sperl, M.; Tartaglia, P.; Voigtmann, T.; Zaccarelli, E. *Phys. Rev. E: Stat. Phys., Plasmas, Fluids, Relat. Interdiscip. Top.* **2001**, *63*, 011401.
(21) Stober, W.; Fink, A.; Bohn, E. *J. Colloid Interface Sci.* **1968**, *26*, 62.
(22) Bogush, G. H.; Tracy, M. A.; Zukoski, C. F. *J. Non-Cryst. Solids* **1988**, *104*, 95.
(23) van Helden, A. K.; Jansen, J. W.; Vrij, A. *J. Colloid Interface Sci.* **1981**, *81*, 354.
(24) Carnahan, N. F.; Starling, K. E. *J. Chem. Phys.* **1970**, *53*, 600.
(25) Berry, G. C. *J. Chem. Phys.* **1966**, *44*, 4550.
(26) Fetters, L. J.; Hadjichristidis, N.; Lindner, J. S.; Mays, J. W. *J. Phys. Chem.* **1994**, *23*, 619. de Gennes, P. G. *Scaling Concepts in Polymer Physics*; Cornell University Press: Ithaca, NY, 1979.

Table 1. Experimental System[a]

molecular weight (g/mol) [R_g (nm)]^{solvent}	R (nm)	R_g/R	ϕ_c	c_p/c_p^*	scattering method[b]
1.32×10^4	50 ± 3	0.061	0.42 ± 0.01	0	1−3
[3.03]^D			0.42	0.05	1
			0.42	0.07	1
			0.42	0.08	1, 3
			0.42	0.09	1
			0.42	0.095	1
			0.42	0.1	1
[3.50]^T	59 ± 3	0.060	0.40 ± 0.01	0	2
			0.40	0.01	2
			0.40	0.02	2
			0.40	0.03	2
			0.40	0.1	2
			0.40	0.15	2
			0.40	0.2	2
9.94×10^5		0.525	0.08 ± 0.01	0.1	3
[26.3]^D			0.25 ± 0.01	0.1	3

[a] Polymer molecular weight, radius of gyration R_g (determined from static light scattering measurements and appropriate scaling),[26] colloid radius R, size asymmetry ratio R_g/R, colloid volume fraction ϕ_c, reduced polymer concentration, and scattering method for the systems studied are all reported. The colloid radii are $R_1 = 50 \pm 3$ nm and $R_2 = 59 \pm 3$ nm (determined from X-ray scattering and confirmed via DLS and TEM) for all samples. Both the polymers and the colloids were suspended in either decalin (D) or toluene (T). [b] (1) USAXS,[27,28] (2) side-bounce USAXS,[34] and (3) SANS.[28,35]

To investigate the effects of the solvent conditions for the polymer, a third series of experiments were carried out in the good (athermal) solvent toluene using $R = 59 \pm 3$ nm particles and polystyrene of molecular weight $M_w = 1.32 \times 10^4$ g/mol corresponding to $R_g/R = 0.06$. The particle volume fraction was held constant at $\phi_c = 0.40 \pm 0.01$, and c_p/c_p^* was increased. A fluid−gel transition was observed at $c_p/c_p^* = 0.07 \pm 0.003$. All the sample conditions studied are summarized in Table 1.

B. Microstructural Characterization: Theory. The elastic scattering intensity of thermal neutrons and X-rays from a colloidal suspension provides a direct measure of the particle structure factor $S_{cc}(q)$, weighted by the particle form factor $P_{cc}(q)$, the absolute scattering length density difference $\Delta\rho$ of the scatterer from the solvent, and the number of scatterers in a volume V_p:

$$I_s = \phi V_p(\Delta\rho)^2 P_{cc}(q)\, S_{cc}(q) + B_i \tag{1}$$

Here, B_i is an experimentally determined incoherent scattering term.[27,28] The form factor appropriate for a single homogeneous sphere of radius R is given by

$$P_{cc}^0(q, R) = \left\{\frac{3[\sin(qR) - qR\cos(qR)]}{(qR)^3}\right\}^2 \tag{2}$$

$$q = (4\pi n_s/\lambda)\sin(\theta/2)$$

where q is the scattering vector, θ the scattering angle, λ the wavelength, and n_s the refractive index of the medium. The suspensions studied are weakly polydisperse, and the effective form factor can be approximated:

$$P_{cc}(q, R) = \sum_i x_i (r_i/R)^6 P_{cc}^0(q, r_i) \tag{3}$$

Here, x_i is the number fraction of species i and $R = D/2$ is the mean particle radius. For a narrow Gaussian size distribution, the summation can be replaced by the integral

$$P_{cc}(q, R) = \frac{1}{2\pi\sigma}\int_0^\infty \exp\left[-\frac{(r-R)^2}{2\sigma^2}\right] P_{cc}^0(q, R)\left(\frac{r}{R}\right)^6 dr \tag{4}$$

where σ is the variance of the size distribution. The static structure factor $S_{cc}(q)$ provides an ensemble measure of the spatial correlation between particles.

At the relatively small values of the wavevector relevant to our experiments, the measured intensities are dominated by the scattering from the larger colloid particles, which have a greater scattering cross section than the polymer.[9,29] Hence, the subscript nomenclature (cc) denotes the colloid−colloid scattering intensity and structure is henceforth dropped.

The experimental static structure factor is determined by dividing the normalized total scattered intensity by the single particle scattering function in the limit of vanishing ϕ_c [where $S(q) \rightarrow 1$ by construction]. To prevent the introduction of artifacts into the data, a high density of points or a narrow angular resolution (Δq) is required. The quantitative measurements of the incoherent scattering and prefactor terms in eq 1 are obtained from an analysis of the Porod region (where the scattering intensity decays as q^{-4}) via a linear plot of $I(q)q^4$ versus q^4 to extract a slope and intercept, respectively.[30]

C. Microstructural Characterization: Experiment. USAXS measurements were made at the UNICAT facility on the 33-ID line, Advanced Photon Source facility at Argonne National Laboratory. The instrument utilizes a Bonse−Hart camera using Si(111) optics with an available q range of 10^{-4}−1 Å^{-1} and a q resolution of $\Delta q = 1.5 \times 10^{-4}$ Å^{-1} ($\lambda = 1.54$ Å). The beam size is 0.4-mm vertical × 1.5-mm horizontal, through which approximately 2×10^{13} photons/sec are incident at 10 keV. The incident collimated X-ray beam intensity was measured throughout the duration of the experiment. The scattered beam was analyzed by a rotating Si(111) channel cut crystal and measured by a photodiode detector. Each scan was taken on 1-mm-thick samples sealed with Kapton polyimide film windows for about 30 min.[31] The linear photodiode detector operates over a 10-decade intensity range with a slit length of $Q_h = 0.05$ Å^{-1} (in q space). The measured intensity at a given wavevector q is averaged over the slit area, resulting in a slit-smeared intensity $I_s(q)$:

$$I_s(q) = \frac{1}{Q_h}\int_0^{Q_h} I_{DS}\sqrt{Q^2 + q^2}\, dQ \tag{5}$$

where I_{DS} is the desmeared intensity and $Q_h = (2\pi/\lambda)(h/L)$. Here, h is defined as the variable along the slit length and L is the sample-to-detector distance (300 mm). The wavelength resolution of the USAXS instrument is $\Delta\lambda/\lambda = 1.5 \times 10^{-4}$, and as such, no wavelength desmearing is necessary.

The small-angle scattering data is corrected for slit-smearing effects using an iterative method described by Lake,[32] which solves the above integral equation over the entire q range and assumes that the slit is uniformly illuminated. To illustrate these geometric effects, the inset plot in Figure 2 shows the scattering intensities for a sample of 100 ± 6 nm diameter sterically stabilized silica particles suspended in decalin at $\phi_c = 0.42 \pm 0.01$, where they behave as hard spheres.[33] Geometric desmearing clearly increases the resolution of the first peak and the periodic scattering profile of single spherical scatterers at higher values of q. To calculate $S(q)$, values of $P(q)$ and $I(q)$ are needed at the same q. This was accomplished by developing an analytic fit (eq 4) to the experimental form-factor data ($\phi_c < 0.03$) such that $P(q)$ could be calculated at all q (inset in Figure 2).

Experiments were also conducted with effective pinhole collimation. The use of side-reflection Si(111) stages effectively

(27) Glatter, O.; Kratky, O. *Small-Angle X-ray Scattering*; Academic Press: New York, 1982.
(28) Lindner, P.; Zemb, T. *Neutron, X-Ray, and Light Scattering*; Elsevier: New York, 1991.
(29) Apfel, U.; Horner, K. D.; Ballauff, M. *Langmuir* **1995**, *11*, 3401. Horner, K. D.; Topper, M.; Ballauff, M. *Langmuir* **1997**, *13*, 551. Weiss, A.; Potschke, D.; Ballauff, M. *Acta Polym.* **1996**, *47*, 333.
(30) Wagner, N. J.; Krause, R.; Rennie, A. R.; D'Aguanno, B.; Goodwin, J. *J. Chem. Phys.* **1991**, *95*, 494.
(31) Shah, S. A. Ph.D. Thesis, University of Illinois, Urbana-Champaign, 2003.
(32) Lake, J. A. *Acta Crystallogr.* **1967**, *23*, 191.
(33) Hansen, J. P.; McDonald, I. R. *Theory of Simple Liquids*, 2nd ed.; Academic Press: London, 1986.

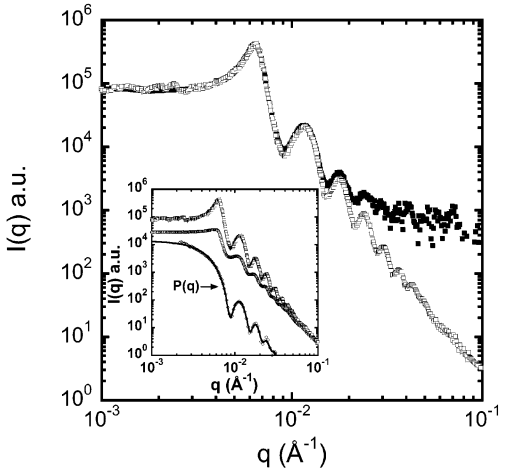

Figure 2. Normalized scattering intensity $I(q)$ in arbitrary units as a function of the scattering angle q for hard-sphere octadecyl silica particles of diameter $D = 100 \pm 6$ nm suspended in decalin at $\phi_c = 0.42 \pm 0.01$. The open symbols are the desmeared data (following the procedure of Lake).[32] The filled symbols are the data taken on the same sample with the pinhole-collimated side-bounce USAXS configuration. The inset compares the experimental desmeared data (squares) of the main plot with the slit-smeared data (circles). Also shown in the inset is the desmeared $P(q)$ (diamonds) fit to eq 4 (solid line).

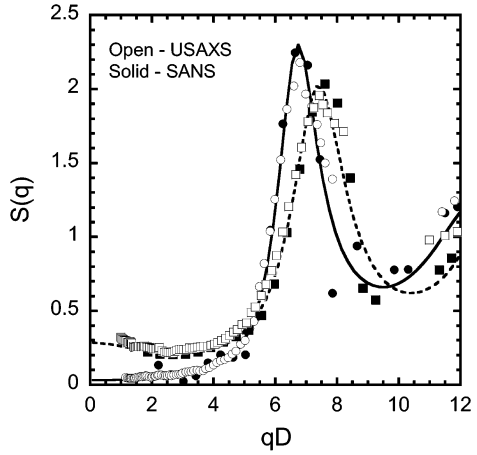

Figure 3. Structure factors as a function of the dimensionless wavevector, qD, for the desmeared USAXS (open symbols) and SANS (filled symbols) data. The data compares two different samples of octadecyl silica particles suspended in decalin at $\phi_c = 0.42 \pm 0.01$: $c_p/c_p^* = 0$ (circles) and $c_p/c_p^* = 0.08$ with $R_g/R = 0.061$ (squares). The solid curve is the Percus−Yevick structure factor for hard spheres, and the short dashed line is the ideal solvent PRISM predictions for $R_g/R = 0.061$.

removes the slit-smearing effects and enables pinhole measurements where unsmeared, rather than slit-smeared, data are obtained.[34] Comparison of the normalized intensity obtained via both techniques allows a rigorous quantitative test of the desmearing algorithm. The hard-sphere data at $\phi_c = 0.42$ shown in Figure 2 compares the desmeared results obtained using the slit-smeared geometry with data from the effective pinhole collimation. Excellent quantitative agreement is found up to $q \sim 0.015$ Å^{-1}, beyond which significant background scattering effects result in poorer quantitative comparisons. This agreement provides justification for the use of the desmearing algorithm to correct for slit smearing in this q range for all subsequent samples, where we probe the structural implications of adding a nonadsorbing polymer to a suspension of model hard spheres.

SANS measurements were made on the 30-m beam line at the National Institute of Standards and Technology.[35] The wavelength of the neutrons was 5 Å with a wavelength resolution $\Delta\lambda/\lambda \sim 0.15$ and a sample-to-detector distance of 15.3 m. The experimental q range was varied from 2×10^{-3}−3×10^{-2} Å^{-1}. The experiments were conducted with circular pinhole collimation. The samples were loaded into stainless-steel sample cell holders with a 1-mm beam path length between 1-in.-diameter quartz windows sealed with Teflon O-rings.

The SANS data is smeared as a result of both angular collimation and wavelength spread. The desmearing routine applied here approximates the resolution function at each q value by a Gaussian function, and the size, spacing of the source and sample apertures, and detector resolution are used to determine the angular component. The algorithm uses a linear regularization method combining a least-squares fit of the data with a minimization of the second derivative of the solution, which results in a nonunique solution for the desmeared intensity.[36] Multiple scattering effects were minimal.

Structure factors are extremely sensitive to the form of $P(q)$. The largest uncertainty in the $P(q)$ determination appears to be the absolute knowledge of q. At q values where dP/dq is large, uncertainties of ±20% are anticipated. These uncertainties can give rise to anomalous values of $S(q)$ near the minima of $P(q)$. For this reason, the $S(q)$ data are often truncated near $qD =$ 8−10 [close to the first minima in $P(q)$]. Details of the scattering techniques employed for the different samples are summarized in Table 1.

Figure 3 shows a comparison of the net structure factor for the conditions where both USAXS and SANS measurements were made: (i) $c_p/c_p^* = 0$ (hard spheres) and (ii) $c_p/c_p^* = 0.08$ and $R_g/R = 0.06$, both at a colloid volume fraction of $\phi_c \sim 0.42$. The two experimental techniques show excellent quantitative agreement over a wide q range with the Percus−Yevick theory[37] for hard spheres (solid curve) as well as the PRISM theory for the polymer−colloid mixture (dotted curve). The comparison shows a high degree of quantitative agreement, which validates the accuracy of both experimental techniques and their respective desmearing algorithms.

III. PRISM Theory

The PRISM theory is a generalization to polymers of the small-molecule RISM theory of Chandler and Andersen[38] based on an interaction site representation of molecules. The formulation of a novel version of PRISM theory to treat the thermodynamics, structure, and phase separation of mixtures of hard spheres and flexible polymers has been discussed in great depth in recent publications,[4,8−11,39] including the detailed review in ref 12. The standard atomic Percus−Yevick closure is employed for particle−particle direct correlations.[37] For polymers, the appropriate closure approximation for $c_{pp}(r)$ depends on the solvent quality, as is discussed elsewhere.[10,12,39] The novel modified Percus−Yevick (mPY) closure is employed for polymer−particle direct correlations.[10−12] The mPY closure properly accounts for, in a self-consistent manner, the nonlocal loss of conformational entropy when a polymer is near the surface of a hard sphere. The PRISM−mPY theory has been shown to correctly predict the qualitative trends, with quantitative or semiquantitative accuracy, of the F−F phase-separation boundaries, the colloid osmotic compressibility, and other

(34) Ilavsky, J.; Allen, A. J.; Long, G. G.; Jemian, P. R. *Rev. Sci. Instrum.* **2002**, *73*, 1660.

(35) Glinka, C. J.; Barker, J. G.; Hammouda, B.; Krueger, S.; Moyer, J. J.; Orts, W. J. *J. Appl. Crystallogr.* **1998**, *31*, 430. Choi, S.-M.; Barker, J. G.; Glinka, C. J.; Cheng, Y. T.; Gammel, P. L. *J. Appl. Crystallogr.* **2000**, *33*, 793.

(36) Barker, J. G. Personal communication.

(37) Percus, J. K.; Yevick, G. J. *Phys. Rev.* ***1958***, *110*, 1.

(38) Schweizer, K. S.; Curro, J. G. *Adv. Polym. Sci.* **1994**, *116*, 319. Schweizer, K. S.; Curro, J. G. *Adv. Chem. Phys.* **1997**, *98*, 1. Chandler, D.; Andersen, H. C. *J. Chem. Phys.* **1972**, *57*, 1930. Chandler, D. *Studies in Statistical Mechanics*; North-Holland: Amsterdam, 1982; Vol. 8, p 274.

(39) Chen, Y. L.; Schweizer, K. S.; Fuchs, M. *J. Chem. Phys.* **2003**, *118*, 3880.

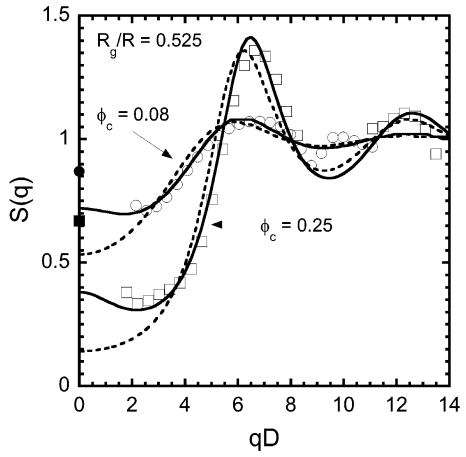

Figure 4. Comparison of the experimental structure factors obtained from SANS for suspensions at two colloid volume fractions, $\phi_c = 0.08$ (open circles) and 0.25 (open squares), at a fixed polymer concentration $c_p/c_p^* = 0.1$ and $R_g/R = 0.525$. The curves are the corrresponding theoretical predictions: Percus−Yevick for hard spheres (dashed) and ideal PRISM−mPY (solid). The osmotic compressibilities, $S(0)$, reported previously[4] for $\phi_c = 0.08$ (filled circles) and 0.25 (filled squares) are also shown for comparison.

thermodynamic properties as functions of R_g/R, the volume fraction, and the solvent quality.[4,8,9] The theory also predicts the collective partial structure factors

$$\hat{S}_{ij}(q) = \rho_i \hat{\omega}_i(q)\delta_{ij} + \rho_i \rho_j \hat{h}_{ij}(q) \qquad (6)$$

where δ_{ij} is the Kronecker delta function. Direct theoretical comparisons of the PRISM theory colloidal structure factors to experimental $S(q)$ data [where $S_{cc}(q) = S(q)$] are made in the next section.

IV. Results

The collective colloidal structure increases as the particle concentration is increased. Two examples of the relatively low particle-volume-fraction behavior are shown in Figure 4 for fixed $R_g/R = 0.525$ and $c_p/c_p^* = 0.1$. As is expected, the first peak in $S(q)$ becomes more prominent with increasing ϕ_c, and the values of $S(0)$ from the light scattering measurements[4] appear as natural extrapolations of the low-q SANS data. These results also indicate that SANS can be used to extract high-quality structure factors where changes substantially smaller than 10% can be discerned; for example, the first peak in $S(q)$ at $\phi_c = 0.08$ is clearly visible at a value of about 1.10.

Also shown in Figure 4 are the hard-sphere fluid PY predictions (dashed lines) and no-adjustable-parameter PRISM−mPY (solid lines) calculations. Small shifts are predicted for the location of the first peak in $S(q)$ upon the addition of the polymer. The PRISM−mPY predictions are in good agreement with the experiment for $qD > 2$, which provided further confidence that the $S(q)$ data are accurate at least to within ±10% near the first peak. For $qD \leq 2$, PRISM−mPY underpredicts $S(q)$, for both the $\phi_c = 0.25$ and 0.08 samples. This provides additional evidence that PRISM underpredicts the magnitude of long-wavelength density fluctuations as the F−F demixing boundary is approached.[4]

The effects on the colloidal structure of increasing c_p/c_p^* are more dramatic at high (fixed) particle volume fractions. A systematic series of such scattering experiments for colloids suspended in both decalin and toluene have been performed. The particle size and polymer molecular weight were chosen to yield the same value of

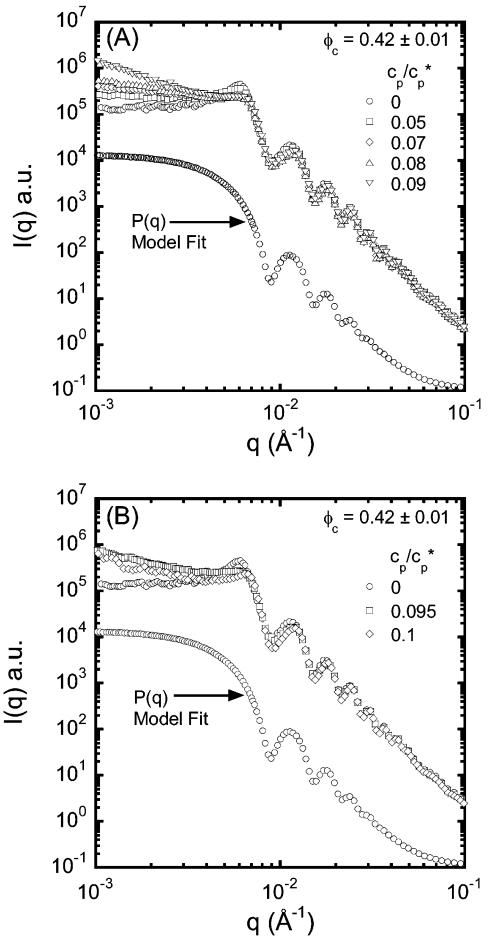

Figure 5. (A) Normalized scattering intensities $I(q)$ as a function of q (Å^{-1}) for the liquid samples in decalin with varying amounts of the polymer quantified by the dimensionless polymer concentration c_p/c_p^*. The colloid volume fraction is fixed at $\phi_c = 0.42 \pm 0.01$, and $R_g/R = 0.061$ where $c_p^{gel}/c_p^* = 0.095 \pm 0.005$. The data are shown for $c_p/c_p^* = 0$ (circles), 0.05 (squares), 0.07 (diamonds), 0.08 (triangles), and 0.09 (inverted triangles). (B) Normalized scattering intensities $I(q)$ as a function of q (Å^{-1}) for gel samples in decalin: $c_p/c_p^* = 0.095$ (squares) and 0.10 (diamonds) for ϕ_c and R_g/R the same as those in part A. The pure hard-sphere result (circles) is also shown. Model fits for $P(q)$ (circles) are shown for comparison.

R_g/R under near-theta (decalin) and athermal (toluene) conditions. Figure 5A shows the desmeared USAXS intensities as a function of the scattering wavevector in decalin and increasing polymer concentration at a fixed size asymmetry ratio of $R_g/R = 0.061$. All samples are in the homogeneous fluid phase at a fixed colloid volume fraction $\phi_c = 0.42 \pm 0.01$. The corresponding reduced structure factors, $S(q)$, as a function of the dimensionless wavevector qD are shown in Figure 6A. There are three basic trends with increasing polymer concentration.

(1) A relatively modest, ∼15% monotonic shift of the location of the first peak of the structure factor ($q^* \sim 0.006$ Å^{-1}) to higher wavevectors as c_p/c_p^* is increased occurred. Physically, this is due to the increasing compression of the local cage by the depletion attractions.

(2) The intensity of the first peak, $S(k^*)$ (where $k^* = q^*D$), serves as a collective local or cage order parameter and varies nonmonotonically with the polymer concentration. $S(k^*)$ initially decreases with the polymer additions, in agreement with a recent experimental study of the reentrant glass transition phenomenon in suspensions of cross-linked microgel colloids.[13] The physical interpretation is that at small polymer concentrations the attractions

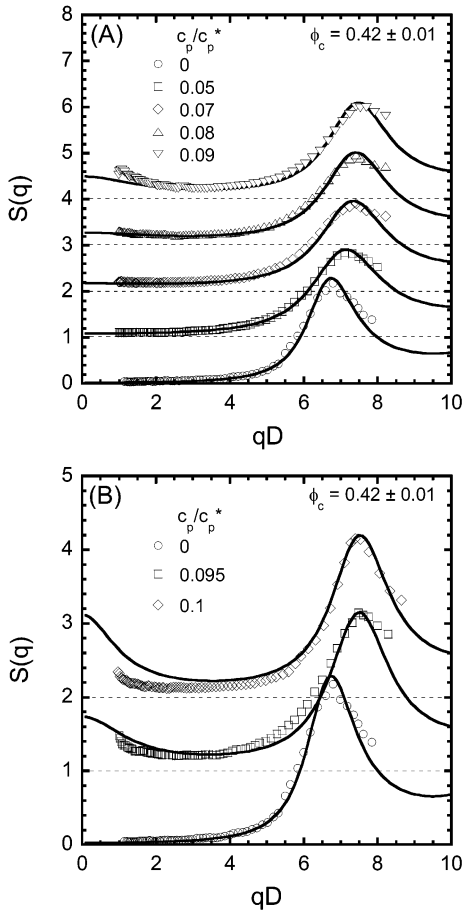

Figure 6. Structure factor as a function of the dimensionless wavevector for samples in decalin with varying amounts of the polymer. The colloid volume fraction is fixed at $\phi_c = 0.42 \pm 0.01$, and $R_g/R = 0.061$. (A) Liquid samples: $c_p/c_p^* = 0$ (circles), 0.05 (squares), 0.07 (diamonds), 0.08 (triangles), and 0.09 (inverted triangles). (B) Gel samples: $c_p/c_p^* = 0.095$ (squares), 0.1 (diamonds), and, as a reference, $c_p/c_p^* = 0$ (circles). Each subsequent data set is offset by 1 for clarity. The dotted lines show relevant baselines signifying $S(q) = 0$ for each data set. The solid lines are the no-adjustable-parameter ideal PRISM−mPY theory predictions.

between colloids results in heterogeneity on the length scales characterizing the first shell of the particles around a central particle.[12,19,20] This suppresses the cage coherence or, loosely speaking, enhances the local free volume. However, with an increasing polymer concentration, the peak intensity goes through a minimum and then increases by a modest amount until the gel line is reached. The interpretation of this nonmonotonic behavior is that the increasing overall compression of the local cage with more polymer additives becomes the dominant effect, resulting in a local densification of the cage and enhancement of the wide-angle scattering intensity. Also shown in Figure 6A are the no-adjustable-parameter predictions of the PRISM theory (solid curves), which are in near quantitative agreement with all the aspects of the scattering data for $qD > 2$.

(3) As was expected, at low scattering angles there is a monotonic enhancement of the scattering intensity. This represents the thermodynamic manifestation of the depletion attractions, which results in enhanced long-wavelength-concentration fluctuations as a precursor to phase separation (controlled in this case by a "buried" spinodal). The theory remains in good agreement with the experiment, although its quantitative accuracy worsens as $c_p/c_p^* \geq 0.08$. As is also seen for the $R_g/R = 0.525$ system in Figure 4, PRISM underpredicts $S(q)$ at small wavevectors.

Above $c_p/c_p^* = 0.09$, an abrupt gel transition occurs where the sample viscosities display divergent behavior and the suspensions develop long mechanical relaxation times (cessation of flow). The F−F spinodal boundary predicted by the PRISM theory in decalin is at $c_p/c_p^* = 0.12$, roughly 30% higher than that of the gel boundary. This demonstrates that gelation is *not* the result of quenching our samples into an unstable two-phase region of the equilibrium phase diagram.[33] This conclusion is supported by the $S(0)$ osmotic-compressibility studies reported earlier.[4]

The USAXS scattering functions and corresponding structure factors for two gel samples just into the gel state ($c_p/c_p^* = 0.095$ and 0.1) are shown in Figures 5B and 6B. The hard-sphere data are also shown for comparison. The height and location of the wide-angle scattering peak remain nearly constant as the polymer concentration changes in the gel state. A similar local structural insensitivity to the strength of weak short-range adhesive hard-sphere attractions in thermoreversible gels has been previously reported by Rueb and Zukoski.[40] The excellent agreement with PRISM−mPY predictions indicates that the local structure on the particle size scale is essentially the same as that in the equilibrium fluid. Curiously, in the gel the magnitude of the first peak remains comparable to its value for the pure hard-sphere suspension, which is also in agreement with the prior study of Rueb and Zukoski.[40] This observation suggests that the particles are locally more dense, resulting in a more rigid structure able to transmit stress.[41]

The lower angle scattering intensity ($1 \leq qD \leq 3$) does change in the gel state and is significantly *lower* than that for the liquid samples. The latter trend is opposite of the PRISM predictions and what is expected on the basis of the increasing depletion attractions under equilibrium conditions. Hence, nonmonotonic changes (corresponding with an abrupt departure from the equilibrium theory) of the intensity with the polymer concentration are again seen but this time signal the *falling out* of the equilibrium on length scales on the order of two colloid diameters and larger as the gel boundary is traversed. The ability to draw such a clear conclusion is contingent on having both experimental and accurate theoretical structural information.

Figure 7A shows the structure factors under athermal good solvent conditions in the homogeneous fluid phase. The trends with increasing polymer concentration are qualitatively identical to those observed for the near-theta solvent decalin. The level of quantitative agreement with the PRISM theory is comparable to that in the decalin case. The corresponding structure-factor data in the gel state are shown in Figure 7B. In contrast to the decalin experiments, states deep in the gel are probed up to $c_p/c_p^{gel} \approx 3$. To within the experimental uncertainties associated with the limited angular resolution at the lowest q values ($\Delta q \sim 1.5 \times 10^{-4}$ Å^{-1}), the intensity for $qD < 1-2$ increases strongly in a manner not correlated with the predicted dependence on c_p/c_p^* and proximity to an equilibrium spinodal boundary. The form of the low-angle-wavevector dependence is roughly q^{-4} for all gel samples. Curiously, $S(q)$ for $qD \sim 2-3$ is essentially constant in the gel for all values of c_p/c_p^* examined. Analogous to the measurements made under near-ideal solvent conditions,

(40) Rueb, C. J.; Zukoski, C. F. *J. Rheol.* **1997**, *41*, 197.
(41) Dinsmore, A. D.; Weitz, D. A. *J. Phys.: Condens. Matter* **2002**, *14*, 7581.

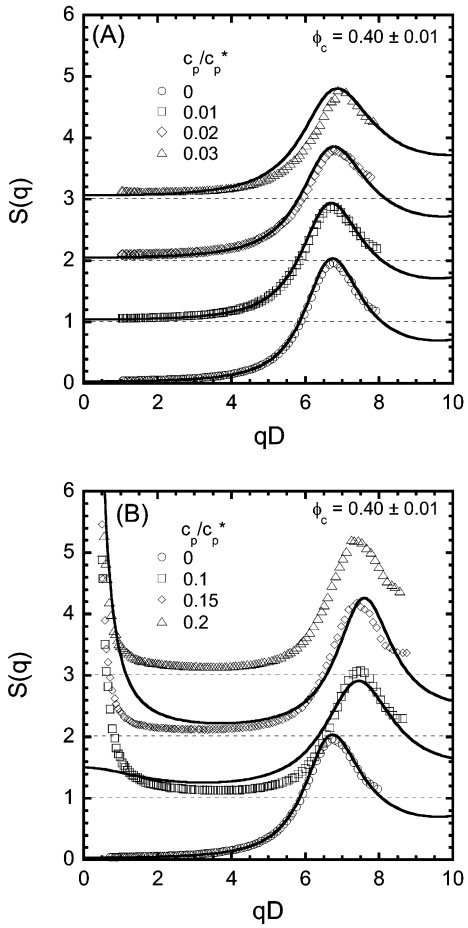

Figure 7. Structure factor as a function of the dimensionless wavevector for samples in toluene with varying amounts of the polymer. The colloid volume fraction is fixed at $\phi_c = 0.40 \pm 0.01$, and $R_g/R = 0.06$. (A) Liquid samples: $c_p/c_p^* = 0$ (circles), 0.01 (squares), 0.02 (diamonds), and 0.03 (triangles). (B) Gel samples: $c_p/c_p^* = 0$ (circles, shown for reference), 0.1 (squares), 0.15 (diamonds), and 0.2 (triangles). Each subsequent data set is offset by 1 for clarity. The dotted lines show relevant baselines where $S(q) = 0$ for each data set. The solid lines are the athermal PRISM−mPY theory predictions.

the local structure of the gels is also relatively insensitive to the strength of the depletion attractions over the range $1 \leq c_p/c_p^{gel} \leq 3$. As was expected, the gel structural data show significant deviations from the PRISM predictions, which again establishes the nonequilibrium nature of the structural correlations even on the cage length scale. Under athermal solvent conditions, the depletion-attraction effect is weaker, and the PRISM theory predicts that the F−F spinodal lies at a higher value of the reduced polymer concentration of $c_p^{spin}/c_p^* \approx 0.15$. No theoretical calculation is shown for the $c_p/c_p^* = 0.2$ case because it lies inside the spinodal region.

V. Discussion and Summary

We have presented a systematic small-angle scattering study of the influence of the depletion attractions on the collective colloidal structure in polymer−particle suspensions. Roughly 1 order of magnitude variation in the length scale has been probed, from ∼1−10 particle diameters. The majority of our results are for a high particle volume fraction of ∼ 40% and a size asymmetry ratio corresponding to colloids about 17 times larger than the flexible polymer coils. Keeping the latter two system parameters fixed allows an unambiguous study of the influence of both the polymer concentration and solvent quality

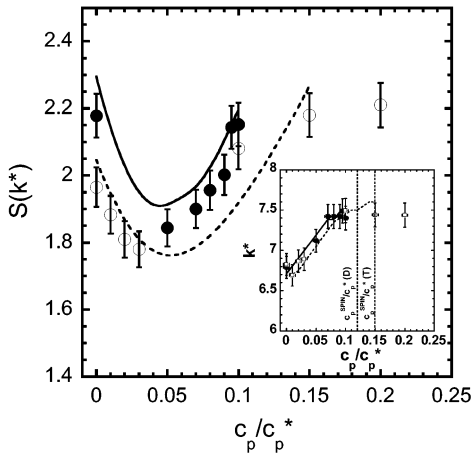

Figure 8. Structure factor at the position of the first peak, $S(k^*)$, as a function of c_p/c_p^* for $R_g/R \sim 0.06$ samples in decalin (solid symbols) and toluene (open symbols) for both the liquid and the gel states. Experiments in decalin (D) are at $\phi_c = 0.42 \pm 0.01$ and in toluene (T) at $\phi_c = 0.40 \pm 0.01$. The curves are the corresponding PRISM−mPY predictions for the ideal (solid) and athermal good solvency (dashed) conditions. The inset shows the position of the first peak k^* as a function of the reduced polymer concentration. The locations of the PRISM−mPY spinodals are shown for both solvents as the vertical dotted lines at the indicated values of c_p^{spin}/c_p^*.

(effective polymer−polymer interactions) on the depletion-driven structural changes. The relevant values of the reduced polymer concentrations are small, $c_p/c_p^* \ll 1$, and measurements in both the homogeneous fluid phase and the nonergodic gel have been performed.

Figure 8 summarizes the influence of the depletion attractions on the two primary structural features on the local cage scale. In the homogeneous fluid phase, the characteristic cage length scale, $2\pi/k^*$ (where $k^* = q^*D$), decreases by ∼15% with increasing polymer concentration and appears to eventually saturate. The cage order parameter $S(k^*)$ is a nonmonotonic function of polymer concentration. This feature plays a crucial role in the depletion-driven "colloid glass melting" phenomenon.[14,19] Excellent agreement with the no-adjustable-parameter predictions of PRISM−mPY theory is found for k^* and $S(k^*)$ under both ideal and athermal solvent conditions. The degree of nonmonotonic behavior, and more generally even the qualitative shape of the $S(k^*)$ versus c_p/c_p^* curve, is predicted by PRISM theory to depend sensitively on the volume fraction and size asymmetry ratio.[12]

Good agreement between experiment and theory is also found on intermediate length scales (Figure 9). A modest quantitative underprediction of the scattering intensity at the lowest wavevectors and highest polymer concentrations (Figures 4, 6A, and 7A) is consistent with the conclusions drawn from prior theory−experiment comparisons for phase diagrams and osmotic compressibilities.[4,8,9]

Upon crossing the gelation boundary, k^* and $S(k^*)$ appear to arrest, implying an insensitivity of the gel cage structure to the polymer concentration. For both the decalin and toluene systems, $S(k^*)$ in the gel approaches a value close to the predicted equilibrium value at the F−F spinodal boundary. Whether this correspondence is an "accident" is not known at present. The longer-range (small-wavevector) fluctuations in the gel also appear to be relatively insensitive to changes in the polymer concentration (see Figure 7B).

A pronounced departure of the equilibrium theory predictions from experiment in the gel can be seen at

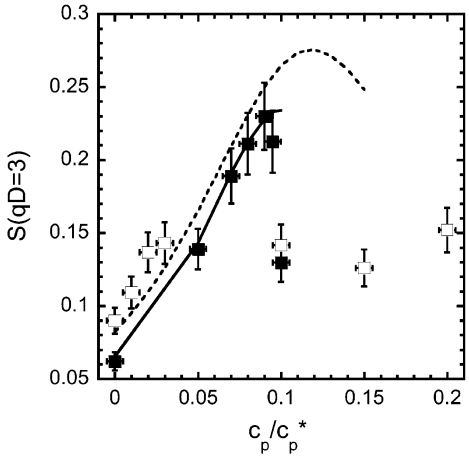

Figure 9. Structure factor at the dimensionless wavevector $qD = 3$ as a function of c_p/c_p^* in decalin (filled symbols) and toluene (open symbols) at a fixed value of $R_g/R \sim 0.06$. The data for both the liquid and the gel samples are included. The curves are the corresponding PRISM−mPY predictions for the ideal (solid) and good (dashed) solvent conditions.

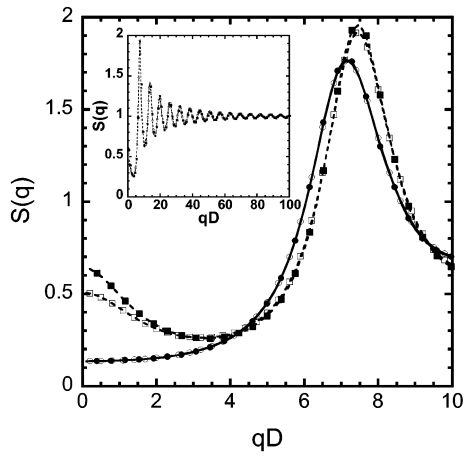

Figure 10. PRISM−mPY calculations of the colloidal structure factor under the ideal (filled symbols) and athermal (open symbols) solvent conditions for a fixed $R_g/R = 0.06$ and $\phi_c = 0.40$. The results for two reduced polymer concentrations are shown: $c_p/c_p^* = 0.06$ (circles) and 0.1 (squares). The inset shows the same structure factors for the $c_p/c_p^* = 0.1$ case, but they are plotted out to very large wavevectors where $qR_g \sim 2\pi$.

longer length scales beginning at ∼2−3 particle diameters. Figure 9 highlights the excellent quantitative agreement with the liquid-state predictions at $qD \sim 3$ up to the gelation boundary, followed by an abrupt departure in the direction of the suppressed concentration fluctuations in the gel. The experimental data imply an abrupt freezing of the intermediate scale structure. Hence, the departure of the scattering data from the equilibrium theory predictions provides a novel signature for detecting or defining gelation, which is complementary to more common measures such as visual inspection or changes in the viscoelastic response.

It is interesting to compare our results with those in the prior studies of Rueb and Zukoski[40] of the gelation of octadecyl silica particle suspensions induced by cooling. In the cooling experiment, the gel can be formed in situ starting with a hard-sphere mixture, and cooling deep within the gel allows the effects of shear to be studied. These experiments revealed that even deep in the gel state the first peak in the structure factor changed little from the hard-sphere suspension behavior. In addition, steady shear had no effect near the first peak in $S(q)$, although the dynamic moduli were strongly affected. The amplitudes of the low q fluctuations increased with shear, eventually saturating at a sufficiently high rate. In our present studies, the samples are exposed to high shear rates during both the mixing of the polymer−particle suspensions and loading into the scattering cell. As a result, we expect our samples to lie closer to the high-shear-rate results reported by Rueb and Zukoski[40] than the gels formed quiescently upon lowering the temperature.

Figures 8 and 9 also summarize the influence of the solvent quality on the local structural changes at a *fixed* size asymmetry ratio. The modest vertical offsets are attributed to small differences in the experimental volume fractions ($\phi_c = 0.4$ in toluene and 0.42 in decalin). This statement is strongly supported by PRISM calculations, which find that if the size asymmetry, volume fraction, and reduced polymer concentration are all fixed then the differences between athermal and ideal solvents for the local cage structural properties are less than 4%, a likely immeasurably small difference. An example of the theoretical results that address this point is given in Figure 10.

The insensitivity of the cage scale correlations to solvent quality should be contrasted with the strong and qualitative influence of solvent quality on the F−F phase separation boundaries and osmotic compressibilities found in prior experimental studies, which were successfully accounted for by PRISM theory.[4,8,9] For ideal solvents, the thermodynamic consequences of depletion-attraction effects are stronger and depend in a qualitatively different fashion on the size asymmetry than do those for the analogous athermal solvent system. For ideal solvents at $\phi_c = 0.40$, equilibrium F−F phase boundaries occur at lower values of c_p/c_p^* as R_g/R increases.[4,39] However, for good solvents the phase boundaries at $\phi_c = 0.40$ occur at larger c_p/c_p^* as R_g/R increases.[8,10,12] This behavior is reflected in the experimental and PRISM results for the osmotic compressibility.[4,9]

There remains the experimental observation that the gel boundary in athermal solvents occurs for a significantly lower reduced polymer concentration than that in ideal theta solvents. Hence, gelation is "easier" for suspensions where the polymers mutually repel (i.e., $c_p^{T-gel} < c_p^{D-gel}$), opposite to the trend for F−F phase separation (i.e., $c_p^{T-spin} > c_p^{D-spin}$).[4,8,9] These facts establish the irrelevance of equilibrium long-wavelength-colloidal-concentration fluctuations (buried spinodal) for the gelation process, at least for the systems we study where gelation occurs directly from the homogeneous fluid phase and not in a metastable two-phase region of the phase diagram.[2] In addition, the experimentally measured amplitude of the long-wavelength-concentration fluctuations in the gel state appear insensitive (to a first approximation) to changes in the polymer concentration. Hence, such low q effects, even if they are of a nonequilibrium origin, may not be strongly correlated with the viscosity and mechanical strength of the gels, which do depend on the polymer concentration.[42] Also, because the cage structure is nearly independent of solvent quality, this suggests that the colloidal correlations on the particle diameter (or cage) scale are not critical to the gelation process.

(42) Goodwin, J. W.; Hughes, R. W.; Kwaambwa, H. M.; Reynolds, P. A. *Colloids Surf., A* **2000**, *161*, 339. Patel, P. D.; Russel, W. B. *J. Rheol.* **1987**, *31*, 599. Buscall, R.; McGowan, I. J.; Mumme-Young, C. A. *Faraday Discuss. Chem. Soc.* **1990**, *90*, 115.

The above deductions concerning the relationship between structure and gelation are consistent with the ideas of MCT. This theory argues that, especially at the high colloid volume fractions of interest, a crucial process is the formation of effectively permanent "physical bonds" between colloids and the particle localization is on a length scale controlled by the range of the depletion attraction.[19,20] For our system, the latter corresponds to wavevectors $qD \sim 2\pi(R/R_g) \sim 100$, far beyond where experiments can be performed. Hence, a direct experimental determination of whether the system is still in equilibrium in the gel on such small length scales, and any influence of the solvent quality, is not possible. The theoretical equilibrium structure factors on the polymer length scale are shown in the inset of Figure 10 for both the athermal and the nearly ideal cases. The subtle differences are too small to quantify. Indeed, the differences between the athermal and the near ideal solvent cases are very small on all length scales for the specific system studied, despite the fact that $c_p/c_p^{spin} = 0.83$ ($c_p/c_p^* = 0.1$) for the ideal solvent system. These combined experimental and theoretical results raise the question as to whether the observed influence of the solvent quality on gelation may be due to primarily dynamical effects, such as hydrodynamic interactions and their dependence on the solvent conditions and structure of the grafted chains on the colloid surface.

This paper has focused on demonstrating the effectiveness of USAXS to determine the structure factors in dense equilibrium suspensions and the usefulness of PRISM−mPY theory for predicting the structure in depletion-attraction systems. Detailed analysis of the low-q behavior of $S(q)$ in the gel region lies beyond the scope of this paper and is deferred to a future publication.[43] Hence, we conclude by only making a few comments on this aspect.

It is of interest to compare our gelation results with prior studies at low particle volume fractions (typically <10%), where the power-law increase in the scattering intensity at low q is taken as an indication of the formation of fractal clusters.[3,44] Gelation is argued to occur when the fractal clusters begin to jam or stick to form a space-spanning network. In contrast, our high-volume-fraction decalin suspensions, even very close to the gel boundary ($c_p/c_p^{gel} \sim 0.95$), show structure factors that are in quantitative agreement with the equilibrium liquid state theory. The large increases in $S(q)$ at low q in the gel potentially have at least two origins. First, they may be due to "cluster" formation or "heterogeneities". Second, the upturn in $S(q)$ at low q within the gel may arise (at least partially) from the equilibrium concentration fluctuations as the F−F spinodal boundary is approached. This explanation appears unlikely as a result of the apparent freezing of the structural correlations for $c_p \geq c_p^{gel}$.

Acknowledgment. The authors thank P. R. Jemian and J. Ilavsky for advice and support in gathering USAXS data at the synchrotron facility at Argonne National Laboratory. The UNICAT facility at the Advanced Photon Source (APS) is supported by the University of Illinois at Urbana-Champaign, Materials Research Laboratory (U.S. DOE, the State of Illinois-IBHE-HECA, and the NSF), Oak Ridge National Laboratory (U.S. DOE under contract with UT-Battelle LLC), National Institute of Standards and Technology (NIST; U.S. Department of Commerce), and UOP LLC. The APS is supported by the U.S. DOE, Basic Energy Sciences, Office of Science under Contract No. W-31-109-ENG-38. In addition, we thank J. G. Barker, C. Glinka, and M. H Kim for their assistance in gathering and reducing the SANS data at the Center for Neutron Research (CNR) at the NIST in Gaithersburg, MD. We gratefully acknowledge Dr. Matthias Fuchs for many discussions, prior collaborations, and technical assistance with the athermal PRISM calculations. This work was supported by the U.S. Department of Energy Division of Materials Science Grant DEFG02-91ER45439 through the Frederick Seitz Materials Laboratory.

LA020982G

(43) Shah, S. A.; Chen, Y. L.; Ramakrishnan, S.; Schweizer, K. S.; Zukoski, C. F. *J. Phys.: Condens. Matter*, submitted for publication.

(44) Segre, P. N.; Prasad, V.; Schofield, A. B.; Weitz, D. A. *Phys. Rev. Lett.* **2001**, *86*, 6042.